Inverse dynamic load distribution identification for a passenger car tire using vibration responses

H. Devriendt [1,3], F. Naets [1,2], P. Kindt [3], W. Desmet [1,2]
[1] KU Leuven, Department of Mechanical Engineering,
Celestijnenlaan 300, B-3001, Heverlee, Belgium

[2] DMMS Lab, Flanders Make @KU Leuven,
Celestijnenlaan 300, B-3001, Heverlee, Belgium

[3] Tire Vehicle Mechanics,Goodyear Innovation Center* Luxemburg,
Avenue Gordon Smith, L-7750, Colmar-Berg, Leuven

Abstract
The problem of reconstructing the dynamic spatial distribution of transient contact loads exciting a non-linear structure using vibration response measurements is studied. These response measurements are combined with a model that is representative in the frequency range of interest for inverse characterization of the loads. The implementation of two approaches is presented, focusing on the specific time and spatial properties of the input force and the structure. A deterministic inverse technique using impulse responses, together with L-curve Tikhonov regularization, is compared to the stochastic technique of the Augmented Kalman Filter (AKF). A priori knowledge on the spatial distribution of the loads is exploited to enhance the input estimation quality. The presented methodologies are implemented for a high-fidelity full-3D FE model of a passenger car tire rolling with constant velocity on a rough road.

1 Introduction

In automotive industry nowadays, there exists an increasing demand for tires with low noise emission due to market and regulatory trends. The first is related to a shifting customer demand towards more silent and energy-efficient cars. As a consequence, vehicles are produced with more lightweight materials, since this results in lower vehicle weight and lower carbon footprint. Unfortunately, these lightweight materials typically influence the noise behavior negatively. The second aspect involves legal maximum noise emission limits that are being lowered systematically.

Together with noise behavior, tire design typically involves more than 50 performance criteria, such as handling, energy efficiency or wear. As the underlying structure is always the tire, these criteria are highly coupled. Limits or targets on these set out the boundaries and objectives when designing a tire. As this is a very complex task, it is important to know how different design parameters will affect these performance criteria, as well as how different tire designs can be ranked based on these criteria.

One of the important aspects for tire noise is the structure-borne interior cabin noise. This type of noise is typically dominant over the airborne noise in the $0 - 400Hz$ range when driving on a rough road [1], [2]. An important parameter for this type of noise is the dynamic spatial distribution of the contact forces between the tire and the road in the contact patch. These forces give rise to wheel hub reaction forces that are transmitted through the vehicle body to the cabin, generating interior noise. However, the dynamic distribution of these forces is difficult to obtain in practice. One could try to measure it with a dedicated sensor on a prototype, which has been done for rolling on a smooth road [3]. This is very costly and for driving on a rough road, sensors might get damaged. Another approach would be to simulate the tire/road forces using a digital twin of the tire [4],[5]. This comes with the drawbacks of modeling simplifications and computational cost which is typically very high when accurate results with sufficient frequency and spatial resolution are needed for the proposed frequency range.

Therefore, the approach followed in this research is to estimate the forces indirectly. Responses that are easy to measure in practice, such as accelerations, velocities, hub forces, etc are combined with a representative model of the structure. This model should not require extensive pre-processing or tuning. The input forces are then computed in an inverse way. An overview of different approaches for inverse input load characterization is given by Sanchez et al. [6]. Two approaches have been selected: a direct technique, the *Impulse Response Matrix Least-squares deconvolution* [7], [8], and a stochastic technique, the *Augmented Kalman Filter* [9], [10]. Both formulate the dynamics of the structure in the time domain. The first technique computes the response measurements at all time steps within a certain time window at once using a convolution-based input/output model. Subsequently, inputs are computed in such a way that the error norm between the measured and computed measurements at all times is minimized. The second technique formulates the input/output relation of the forces to the measurements with a state/space description. The model updates are performed for each time step incrementally. As it is a stochastic technique, it is possible to quantify the degree of uncertainty one has over the model or the measurements. Predictions for the measurements at the next time step are computed using the model, and these are compared to the actual measurements at that next time step. The inputs are updated in such a way that the uncertainty on the states and inputs is minimized. By doing so, information that is less certain will contribute to a lesser extent to the update of the state and inputs.

The estimation of the tire/road dynamic contact force distribution poses several difficulties. When a high spatial resolution of the contact forces is required, the inputs to be estimated are located in a relatively small area of the full structure. So, the difference in response to several closely spaced loads on the structure can be small, especially far away from the excitation zone (being the contact patch). Moreover, the modal density of a tire in the frequency range of interest can be significant, resulting in a model with many degrees of freedom to be used. The estimation accuracy of the two approaches are compared for the identification of external loads on a simple digital twin of a tire. The details of both methods are given in section 2. The used tire model is presented in section 3, and the numerical experiment comparing the two approaches is given in section 4.

2 Inverse load reconstruction techniques

Two time-domain inverse load reconstruction techniques have been chosen to give an estimate of the dynamic spatial distribution of the tire/road contact forces. Formulating the reconstruction problem in the frequency domain has shown to cause numerical difficulties resulting in noise amplification and inversion problems, see the work of Vercammen[1]. A priori assumptions on the properties of the force distribution were applied for improving the conditioning of the inverse problem. The rationale for formulation in the time domain is that the contact forces do not reach a steady-state regime after some time but remain transient. In addition, it is exactly this transient response that is of interest for identification of the exact location of the excitation. In this transient phase, the traveling waves from excitations in the contact patch are still traceable as they travel through the tire. Moreover, the resulting response is not yet fully modal, which would make the localization of the force very difficult as most modeshapes under $400Hz$ show little variation in the small excitation area. This exact excitation location is of interest when reconstructing the spatial distribution of the forces. The first technique is a Least-Squares computation of the full time signal using an Impulse Response Matrix (IRM), whereas the second is a time-stepping approach, namely the Augmented Kalman Filter (AKF).

2.1 Impulse response matrix deconvolution

For a linear system, initially at rest, the response in a Degree Of Freedom (DOF), $\mathbf{y}(t)$, can be expressed as the convolution product of the input forces $\mathbf{u}(t)$ and the response at that DOF to Dirac impulse excitations applied at each input location separately $\mathbf{H}(t)$:

$$\mathbf{y}(t) = \int_0^t \mathbf{H}(t-\tau)\mathbf{u}(\tau)d\tau \tag{1}$$

The idea expressed here is that, since the model is linear, the response to a load time profile can be broken down into the sum of the responses to impulsive excitations at each time τ scaled with the actual load amplitude $\mathbf{u}(\tau)$.

Next, this equation describing the continuous relation between a force at an input location u_i, $i = 1 \dots p$ and a measurement at a response location y_j, $j = 1 \dots k$ is repeated for all excitation-response combinations. For responses sampled at discrete points in time, a discretized version of the continuous convolution integral is needed:

$$\begin{bmatrix} \begin{Bmatrix} y_1 \\ \vdots \\ y_k \end{Bmatrix}_0 \\ \vdots \\ \begin{Bmatrix} y_1 \\ \vdots \\ y_k \end{Bmatrix}_n \end{bmatrix} = h \begin{bmatrix} \mathbf{H}_0 & 0 & \dots & 0 \\ \mathbf{H}_1 & \mathbf{H}_0 & \dots & 0 \\ \vdots & \vdots & \ddots & \vdots \\ \mathbf{H}_n & \mathbf{H}_{n-1} & \dots & \mathbf{H}_0 \end{bmatrix} \begin{bmatrix} \begin{Bmatrix} u_1 \\ \vdots \\ u_p \end{Bmatrix}_0 \\ \vdots \\ \begin{Bmatrix} u_1 \\ \vdots \\ u_p \end{Bmatrix}_n \end{bmatrix} \tag{2}$$

The adopted method in this work assumes that responses to the excitation to be computed and to the impulse forces are sampled at the same rate. If this is not the case, a slightly different formulation of the IRM matrix is needed [11].

Key for this method is to obtain the time-domain Impulse Response Functions (IRF) for each input/measurement combination. In theory, a Dirac impulse is required as reference excitation, being an infinitesimally short pulse in time, which is not realizable in practice. So, an approximation for these can be obtained either through simulation, analytically or experimentally. In this work, IRFs are computed based on a numerical simulation. Therefore, a model is needed that is capable of accurately computing the response to such an approximate Dirac impulse force applied at $t = 0$. This can be modeled by application of a unit impulsive force that is constant during the first timestep. However, this is not an infinitely short impulse. In experiments, especially when using hammer excitation measurements, applying such an infinitely short impulse is technically even less feasible. So, the time-discretized convolution formulation is altered by using so-called *quasi-impulse loads* u^{QI}. In that approach, the impulse responses are the measured responses to a finite impulse excitation, and a transformation of the inputs to Dirac impulse inputs is performed. This is valid, provided it is possible to express the purely impulsive loads in terms of the actual applied load time profiles. Details can be found in the work of Jankowski [7]. Using quasi-impulse excitations acts as a low-pass filter on the results, suppressing high-frequent noise.

2.1.1 The Impulse Response Matrix-Least Squares algorithm (IRM-LS)

In order to obtain dynamic results with frequency resolution up to $400-450Hz$, a large number of time steps are necessary. This makes the system to be inverted a lot larger and reduces its conditioning. So, a reasoning similar to the one of Kazemi Amiri [12] is used here for construction of an *Augmented impulse response matrix*. It is thereby assumed that the unknown loads can be linearly interpolated between sampled time steps, and that the IRFs can be sampled at higher rate. If the latter is not possible, one could also use (linear) interpolation between IRF time samples. Then, the discretized convolution integral is computed by adding contributions at all sub-steps in between the time samples. See Figure 1. In this way, a higher sampling rate can be maintained without increasing the size of the problem.

So, the discretized convolution response at a time t_K being:

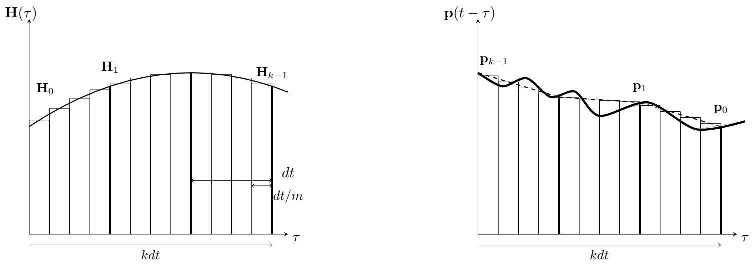

Figure 1: Augmented impulse response with 4 sub-steps (left) and augmented input load (right)

$$\mathbf{y}_K = h \sum_{i=0}^{K} \mathbf{H}_{K-i} \mathbf{u}_i \tag{3}$$

is now replaced by assuming the impulse responses $\mathbf{H}_i$ and inputs $\mathbf{u}_i$ are not constant anymore, but can vary within a time step in a number of sub-steps M. The i-th contribution to the convolution integral is not anymore $\mathbf{H}_{K-i}\mathbf{u}_i$, but is approximated as:

$$\frac{1}{M} \sum_{m=1}^{M} \mathbf{H}_{K-i+m/M} \left\{ \frac{m}{M} \mathbf{u}_i + (1 - \frac{m}{M}) \mathbf{u}_{i+1} \right\} \tag{4}$$

Terms pertaining to $\mathbf{u}_i$ and $\mathbf{u}_{i+1}$ are then arranged properly, resulting in combinations of the IRF sub-steps in a term $\mathbf{H}^{aug}_{K-i}$.

The resulting discretized system of equations using the Augmented Impulse Response Matrix and quasi-impulsive loads $\mathbf{u}^{QI}_i$ is then:

$$\begin{bmatrix} \begin{Bmatrix} y_1 \\ \vdots \\ y_k \end{Bmatrix}_0 \\ \vdots \\ \begin{Bmatrix} y_1 \\ \vdots \\ y_k \end{Bmatrix}_n \end{bmatrix} = h \begin{bmatrix} \mathbf{H}^{aug}_0 & 0 & \dots & 0 \\ \mathbf{H}^{aug}_1 & \mathbf{H}^{aug}_0 & \dots & 0 \\ \vdots & \vdots & \ddots & \vdots \\ \mathbf{H}^{aug}_n & \mathbf{H}^{aug}_{n-1} & \dots & \mathbf{H}^{aug}_0 \end{bmatrix} \begin{bmatrix} \begin{Bmatrix} u^{QI}_1 \\ \vdots \\ u^{QI}_p \end{Bmatrix}_0 \\ \vdots \\ \begin{Bmatrix} u^{QI}_1 \\ \vdots \\ u^{QI}_p \end{Bmatrix}_n \end{bmatrix} \tag{5}$$

In order to solve this equation, a least-squares solution is computed. So, this can be seen as the Linear Least Squares (LLS) technique for the particular case of a system being initially at rest. This LLS technique is used in a large number of studies, see e.g.[13].

2.1.2 Regularization

As already stated in Section 1, the solution typically suffers from ill-conditioning. Specifically, for the application of reconstructing dynamic loads close together in the tire footprint, there are different aspects that add to the ill-conditioning. First of all, the responses at a certain location due to impulsive loads applied at different but closely-spaced locations within the contact patch will be almost the same if the dimensions of the patch are much smaller than the wavelengths of the traveling waves in the frequency range of interest. Second, the measured responses from the input load and the IRF have sensor noise added to the signals. Note that some ill-conditioning is already mitigated by using the interpolated IRM and quasi-impulsive loads.

In order to cope with these issues, Tikhonov Regularization is used [14], where the actual system of equations to solve in a least-squares sense is:

$$min_u \left\{ \|\mathbf{y} - \mathbf{H}_{aug}\mathbf{u}\|^2 + \lambda^2 \|u\|^2 \right\} \tag{6}$$

Formally, this technique adds the constraint that the solution norm of 5 should be small. The importance of this imposed constraint is expressed through the parameter λ. Its value is chosen using the *L-curve*, which plots the solution norm versus the residual norm for different values of λ, typically an L-shaped curve. The optimal value is the one in the corner or 'elbow' of this L-shape. This ensures a good balancing between limiting the solution norm and the residual norm.

2.2 Augmented Kalman filter

For linear systems, the Augmented Kalman filter can be used for providing unbiased estimates of the unknown inputs at each time step.[15],[16]

In this study, dynamics are modeled using a second-order system. The continuous equations of motion are:

$$\mathbf{M}\ddot{\mathbf{z}}(t) + \mathbf{C}\dot{\mathbf{z}}(t) + \mathbf{K}\mathbf{z}(t) = \mathbf{f}(t) \tag{7}$$

with $\mathbf{z}(t) \in \mathbb{R}^{n_{DOF}}$ the response of the system in each Degree-Of-Freedom (DOF), $\mathbf{f}(t)$ the input forces and $\mathbf{M}$, $\mathbf{C}$ and $\mathbf{K}$ the system mass, damping and stiffness matrices, respectively. In order to limit computational cost, the size of the problem is typically reduced using some projection basis $\mathbf{V} \in \mathbb{R}^{n_{red}}$ with lower dimensionality $n_{red} < n_{DOF}$ than the original system, resulting in a reduced system of equations. Likewise, the forces can be projected onto a lower-order set of force shapes $\mathbf{B}$:

$$\mathbf{z}(t) \approx \mathbf{V}\mathbf{q}(t) \tag{8}$$

$$\mathbf{f}(t) \approx \mathbf{B}\mathbf{u}(t) \tag{9}$$

$$\mathbf{M}^{red}\ddot{\mathbf{q}}(t) + \mathbf{C}^{red}\dot{\mathbf{q}}(t) + \mathbf{K}^{red}\mathbf{q}(t) = \mathbf{B}^{red}\mathbf{u}(t) \tag{10}$$

Next, the system of equations is cast in state-space form. In order to have first order model update equations describing the system dynamics, the state $\mathbf{x}$ is defined as:

$$\mathbf{x} = \begin{bmatrix} \mathbf{q} \\ \dot{\mathbf{q}} \end{bmatrix} \tag{11}$$

Since the Kalman filter models a stochastic process, process and measurement noise are added to the model and measurement equations, respectively. These noise terms, $\mathbf{v}(t)$ and $\mathbf{w}(t)$ are vectors of uncorrelated, zero-mean white noise terms with respective covariances $\mathbf{Q}$ and $\mathbf{R}$. These properties are necessary conditions for the generation of an unbiased estimate. The noise terms are measures of the degree of uncertainty of the different model equations or measurements. This leads to the state-space formulation used in the Kalman Filter:

$$\begin{cases} \dot{\mathbf{x}}(t) &= \mathbf{A}\mathbf{x}(t) + \mathbf{B}\mathbf{u}(t) + \mathbf{w}(t) \\ \mathbf{y}(t) &= \mathbf{C}\mathbf{x}(t) + \mathbf{D}\mathbf{u}(t) + \mathbf{v}(t) \end{cases} \tag{12}$$

In the Augmented Kalman filter framework, the unknown input variables $\mathbf{u}$ are added to the state vector, resulting in an augmented state. For the current application, all inputs will be assumed unknown:

$$\mathbf{x}^* = \begin{bmatrix}\mathbf{x}\\ \mathbf{u}\end{bmatrix} \tag{13}$$

In order to include this augmented state in the state-space formulation, an assumption has to be made on the dynamics of the unknown inputs. In this work, a zero-order *random walk* assumption is used [16]:

$$\dot{\mathbf{u}}(t) = \mathbf{0} + \mathbf{w}_u(t) \tag{14}$$

resulting in following augmented state-space formulation:

$$\begin{cases} \dot{\mathbf{x}}^* &= \mathbf{A}^*\mathbf{x}^*(t) + \mathbf{w}^*(t) \\ \mathbf{y}(t) &= \mathbf{H}^*\mathbf{x}^*(t) + \mathbf{v} \end{cases} \tag{15}$$

with the augmented state-space matrices being:

$$\mathbf{A}^* = \begin{bmatrix}\mathbf{A} & \mathbf{B}\\ \mathbf{0} & \mathbf{0}\end{bmatrix}, \mathbf{H}^* = \begin{bmatrix}\mathbf{C} & \mathbf{D}\end{bmatrix} \tag{16}$$

and the augmented process noise and its covariance:

$$\mathbf{w}^* = \begin{bmatrix}\mathbf{w}\\ \mathbf{w}_u\end{bmatrix}, \mathbf{q}^* = \begin{bmatrix}\mathbf{Q} & \mathbf{0}\\ \mathbf{0} & \mathbf{Q}_u\end{bmatrix} \tag{17}$$

Finally, the continuous equations are time-discretized. For this, the model partial differential equation is discretized using an exponential integration scheme with zero-order hold for the inputs [17]. This results in following system of algebraic equations at time step k:

$$\begin{cases} \mathbf{x}^*_{k+1} = \mathbf{F}^*\mathbf{x}^*_k + \mathbf{w}^*_k \\ \mathbf{y}_{k+1} = \mathbf{H}^*\mathbf{x}^*_{k+1} + \mathbf{v}_{k+1} \end{cases} \tag{18}$$

with the integrated process model matrix F^* and the integrated process covariance matrix $\mathbf{Q}^*_d$ of the noise terms given by[18]:

$$\mathbf{F}^* = \begin{bmatrix} e^{\mathbf{A}\Delta t} & \mathbf{A}^{-1}(e^{\mathbf{A}\Delta t} - \mathbf{I})\mathbf{B} \\ \mathbf{0} & \mathbf{I} \end{bmatrix} \tag{19}$$

$$\mathbf{Q}^*_d = \int_0^{\Delta t} e^{\mathbf{A}\tau}\mathbf{Q}e^{\mathbf{A}^T\tau}d\tau \tag{20}$$

These matrices are then input in the Kalman filter time and measurement update equations for computing the *a priori* extended state estimate $\hat{\mathbf{x}}^{*-}$ and *a posteriori* extended state estimate $\hat{\mathbf{x}}^{*+}$ at each time step:

Time update

$$\hat{\mathbf{x}}^{*-}_{k+1} = \mathbf{F}^*\hat{\mathbf{x}}^+_k \tag{21}$$

$$\mathbf{P}^-_{k+1} = \mathbf{F}^*\mathbf{P}^+_k\mathbf{F}^{*T} + \mathbf{Q}^*_k \tag{22}$$

Measurement update

$$\mathbf{K}_{k+1} = \mathbf{P}_{k+1}^{-}\mathbf{H}^{*T}(\mathbf{H}^{*}\mathbf{P}_{k+1}^{-}\mathbf{H}^{*T} + \mathbf{R}_{k+1})^{-1} \tag{23}$$

$$\hat{\mathbf{x}}_{k+1}^{*+} = \hat{\mathbf{x}}_{k+1}^{*-} + \mathbf{K}_{k+1}(\mathbf{y}_{k+1} - \mathbf{H}^{*})\hat{\mathbf{x}}_{k+1}^{*-}) \tag{24}$$

$$\mathbf{P}_{k+1}^{+} = (\mathbf{I} - \mathbf{K}_{k+1}\mathbf{H}^{*})\mathbf{P}_{k+1}^{-} \tag{25}$$

where $\mathbf{P}_k$ is the state covariance and $\mathbf{K}_k$ the Kalman gain. The optimality of the Kalman filter lies in the fact that the trace of this state error covariance matrix is minimized. Conceptually, the time update computes an estimate of the state with corresponding uncertainty in its covariance for the next time step $k+1$ using the model equations. Then, a correction of this *a priori* estimate is applied by using the measurement taken at timestep $k+1$, yielding *a posteriori* an updated estimate and corresponding covariance. The relative importance of the time and measurement updates are expressed through the relative values of the process and measurement noise covariance terms.

By setting initial values for the state $\hat{\mathbf{x}}_0$ and its covariance $\mathbf{P}_0$, the algorithm is initialized and estimates are computed at each timestep.

3 Tire model

Both presented methodologies in Section 2 require a model that is representative for the application of a tire rolling on a rough road. This model should be linear, easy to obtain and ideally have limited amount of DOFs. This is because of computational time, but also because of the amount of measurements necessary for correct force estimates.

The validated simulation framework developed by De Gregoriis [19] is used for generating reference responses as well as impulse responses and model equations. The framework is a fully predictive 3D, coupled vibro-acoustic, non-linear FE modeling tool for simulating rough road rolling of a tire with constant velocity. Physics are incorporated explicitly by modeling the actual materials and structures that make up the tire and using suitable material and interaction laws. Tire/road contact is modeled explicitly, no assumptions are made regarding properties of the forces or the force spatial distribution. The non-linear dynamic simulation of rolling on a rough road is performed in a computationally efficient way by means of a Multi-Expansion Method (MEM) hyper-reduction scheme [20].

First, the tire is inflated, loaded and brought in rotation on a test drum with smooth road surface in a non-linear static simulation. The model is then linearized around this non-linear state and the deviatoric responses are projected onto a lower-order basis: $\mathbf{z}(t) = \mathbf{z}_0 + \mathbf{V}\mathbf{q}(t)$. The assumption behind this linearization is that tire vibrational displacements are typically limited in amplitude, so the system's displacement-dependent properties will not change significantly. Next, the reduced dynamic equations of motion for rolling on a rough road are solved at each time step by using an implicit generalized-α integrator. Responses are polluted with representative sensor noise, depending on the specific response type.

In order to properly describe the forces in a way that limits the amount of force parameters to be reconstructed, a forward reference simulation of rough road rolling of the linearized model is used to exploit the characteristics of the spatial distribution of the dynamic contact forces. Contact forces are band-pass filtered between $50 - 450Hz$, and based on the spatial distribution of their resulting time-RMS values, Areas of Constant Force (ACF) are defined. These are areas within the contact patch where the forces are assumed to have the same value. The more ACFs used, the better the actual contact force distribution will be described, but this comes with aforementioned drawbacks of inverting a system with a high number of unknown inputs. As the final goal is to have a means of ranking different tire designs, a consideration has to be made between the number of inputs necessary for having a representative distribution representation that is still sufficiently accurate after reconstruction, using limited response measurements.

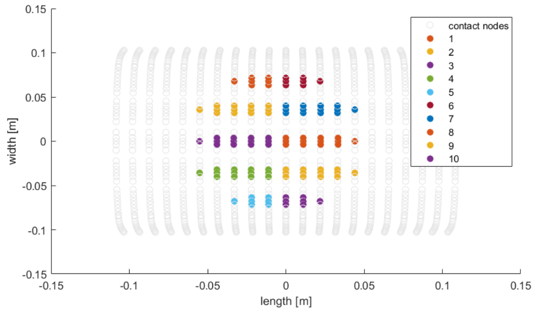

Figure 2: Spatial arrangement of the Areas of Constant Force inside the tire footprint

4 Numerical experiment

Using the framework outlined in the preceding sections, the two force identification techniques are compared for two types of externally applied loads:

- An impulsive load applied in one single ACF
- The force distribution for rough road rolling, expressed as resultant forces constant within the different ACFs

A physically available test tire with only circumferential grooves, a so-called aircraft tire, mounted on a light alloy rim, is modeled using the framework described in Section 2. The size is 225/45R17. Detailed tread modeling for the current application and frequency range can be neglected as this typically only influences the noise at higher frequencies. This assumption yields the advantage of a radially symmetric tire. Construction details are obtained from the tire design, and material data is obtained from material sample tests.

The tire is inflated with an inflation pressure of 2.2 bar and statically loaded on a smooth drum with a vertical load of 5 kN. The drum rotates with fixed angular velocity, bringing the tire into rotation. As no slip is assumed, the drum angular velocity is chosen such that the tire rotates at a constant velocity of 50 kph. This configuration is used as the base state around which to linearize. Originally, the full FE model contains more than 300000 DOFs. The model is reduced in size using a projection basis V containing static and dynamic structural eigenmodes, as well as dynamic acoustic eigenmodes. The input force distribution assumes 10 ACF, covering most nodes where contact occurs during the rough road simulation. See Figure 2.

Reference and impulse response measurements are obtained by running a time simulation on the linearized model with the two aforementioned types of external loads applied. The measurement DOFs for the reconstruction are computed responses from this simulation, polluted with sensor noise. The amplitudes of the noise pollution terms are chosen representative for a typical sensor measuring a certain response type. In this work, measured responses are accelerations using accelerometers with sensor noise covariance of $diag(\mathbf{R}_{acc}) = 10^{-2}(m/s^2)^2$. The measurement locations are all DOFs where an input force can occur, being in each node of the ACFs. Responses are low-pass filtered below $500Hz$. The timestep is $0.2ms$ and total simulation time is $0.15s$.

For the IRF-LS framework, impulse responses are computed numerically by applying a constant smooth road load to the tire and additionally applying impulsive forces in each ACF. Responses are computed using the same parameters for the generalized-α integrator as in the general non-linear simulation. The sampling rate is $0.1ms$. The impulsive force is modeled as the impact force of a hammer with soft rubber tip with cutoff frequency around $500Hz$ [21]:

$$f(t) = \frac{t^{p-1}e^{-t/\theta}}{[(p-1)\theta]^{p-1}e^{1-p}} \tag{26}$$

where p and θ are shape parameters chosen in order to have an impact force with cutoff frequency around

$500Hz$. Furthermore, interpolation using the augmented IRM is applied with 1 substep. Tikhonov regularization is applied using the L-curve for choosing the appropriate λ.

For the AKF, the process noise covariance on the displacement and velocity update equations is put to $\mathbf{Q} = \mathbf{0}$. As the same model is used for the reference measurement and the reconstruction, it is assumed that the uncertainty on the model update equations are negligible compared to the uncertainty on the on the random walk equations for the 10 input parameters. The diagonal values of the latter are chosen to be $10^3 N^2$. This magnitude is chosen several decades larger than the rate of change of the reference forces applied to the model.

In order to avoid long-term drift of the estimated forces using the AKF, dummy displacement measurements are used [22]. These are taken in all nodes inside the contact patch and at several locations spread around the full tire circumference. In order to ensure good force tracking, sensor noise on these dummy displacements is chosen several orders of magnitude larger than their expected values. On the other hand, the value should not be too large in order to still have the stabilizing long-term effect in the Kalman filter. After investigation of the order of magnitudes of the displacements in the dummy response points and subsequent tuning of the value in trial runs, the covariance is chosen at $diag(\mathbf{R}_{dummydisp}) = (10^{-6})^2(m)^2$. Finally, the initial values of the augmented state vector are put to 0, and it is assumed that these initial values are perfectly known, so the corresponding initial covariance matrix is put to a low value: $diag(\mathbf{P}_0) = 10^{-6}$.

4.1 Impulsive force reconstruction

An impulsive load is applied in ACF 2. Comparison of the reconstructed resultant force is shown in figure 3. Both frameworks track the impulsive force quite well, but the AKF estimate does not converge to zero afterwards. As is shown in figure 4, the PSD of the resultant force shows that the AKF filter is more influenced by the modal behavior of the response than the IRM-LS. This is illustrated in figure 6. In addition, the exact localization of the force bump is better for the IRM-LS than for the AKF. See figure 5. Below $200Hz$, the reconstructed loads using the IRM-LS approach shows deviation, as accelerations are lower in magnitude.

So, using the AKF shows more difficulties in tracking the impulsive force in a single patch. The reference measurements are generated using the generalized-α solver, an implicit solver that is known to add numerical damping to a simulation [23]. Typically, this damping is only present at higher frequencies, but it turns out to influence the frequency range of interest as well. This damping effect is not included in the AKF model equations that use an exponential integrator. This causes response mismatch, that is compensated for by changing the input force, since no uncertainty is assumed on the model equations. The IRM-LS estimator uses the full time-response of the same model, but simulated with the generalized-α solver, so this numerical damping effect is included there. Tuning the input covariance did not result in better AKF force estimates. This issue could be resolved using the generalized-α solving scheme as well in the AKF, as was done by Aucejo [21], or by performing the forward time simulations using the exponential integrator.

4.2 Rough road forces on ACF reconstruction

In this experiment, a reference force with a spectrum and amplitude that is more representative for rough road rolling is used. A forward simulation is performed where at each time step, the contact problem is solved explicitly. In a next step, these forces are projected onto the 10 ACF, and in a new simulation, the ACF-projected rough road forces are applied as external forces to the linearized model. Results are shown in figures 7 and 8. The IRM-LS force reconstruction is better than the AKF estimate, both when comparing the resultant force and the estimates per ACF.

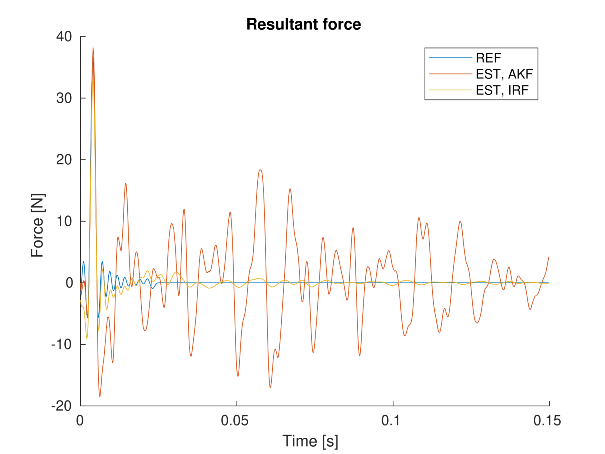

Figure 3: Estimated resultant contact force

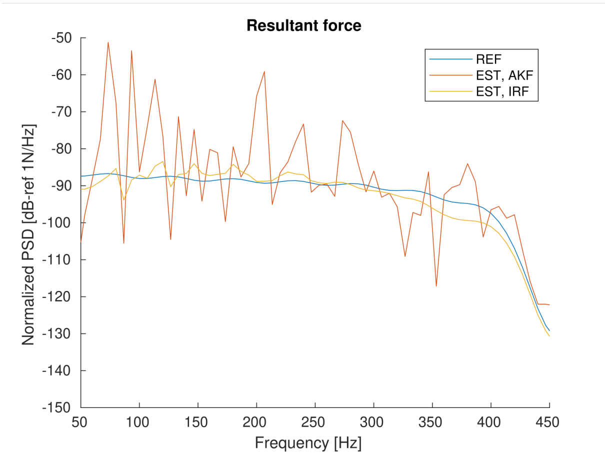

Figure 4: Estimated resultant contact force, PSD

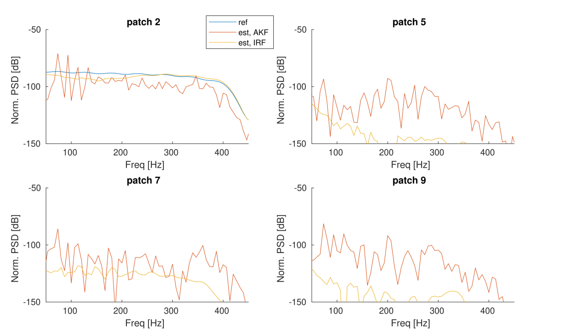

Figure 5: Estimated contact forces for 4 patches, PSD

Figure 6: Comparison of normalized PSD of estimated resultant force with AKF and drive point acceleration

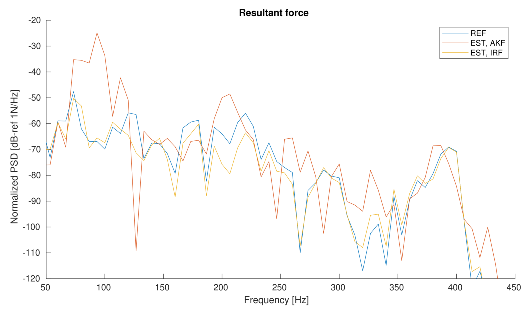

Figure 7: Estimated resultant contact force, PSD

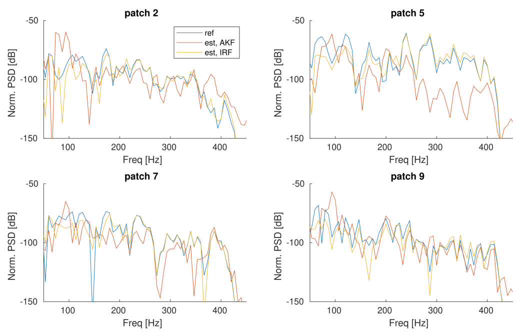

Figure 8: Estimated contact forces for 4 patches, PSD

5 Conclusions

In this work, two methods are compared for the reconstruction of the dynamic force distribution on a structural model of a tire. The goal is to select the best method for estimation of the spatial distribution of the tire-road dynamic contact forces for a tire rolling on a rough road with constant velocity, using responses and a digital twin of the tire. The frequency range of interest is $0 - 500Hz$, where structure-borne interior noise is dominant. The model is generated by linearization of a 3D fully non-linear physics-based FE model around an inflated, loaded and rolling state. Forces are represented by means of Areas of Constant Force, which are areas in the tire footprint where the forces is assumed constant and equally distributed. Both techniques are time-domain techniques, as these are assumed to capture the transient traveling wave behavior resulting from excitations of the tire through the road indents. The first technique is an augmented Impulse Response Matrix Least-Squares load reconstruction with added Tikhonov regularization. The second is the Augmented Kalman Filter with dummy measurements, a stochastic technique. The force reconstruction accuracy comparison is made by reconstructing two different types of load profiles representative for the envisioned application: an impulsive force in one ACF and forces from a contact simulation projected on the ACF set. Accelerations are used as response measurements, and these are obtained using the numerical tire model responses with added sensor noise. The IRM-LS estimator shows better reconstructed resultant forces than the AKF estimator as well as a better reconstruction of the exact spatial distribution of forces input in the system. Moreover, the IRM-LS estimator has the benefit that it could be formulated purely experimentally.The AKF estimation is most deviating from the reference at resonances and anti-resonances. This is the case for the impulsive force, as well as for the rough road forces. Below $200Hz$, the IRM-LS force reconstruction shows increasing deviation from the reference force.

Acknowledgement

The author gratefully acknowledges the European Commission for its support of the Marie Sklowodowska Curie program through the ETN PBNv2 project (GA 721615).

References

[1] W. Vercammen, *Tyre/Road Noise Due to Road Surface Texture Excitations*. Leuven, Belgium: Katholieke Universiteit Leuven, Departement Werktuigkunde, 2017.

[2] L. Hartleip and T. Roggenkamp, "Case study - experimental determination of airborne and structure-borne road noise spectral content on passenger vehicles," *SAE Technical Paper*, vol. 2005-01-2522, 2005.

[3] J. Cesbron, F. Anfosso-Ledee, D. Duhamel, H. Ping Yin, and D. Le Houedec, "Experimental study of tyre road contact forces in rolling conditions for noise prediction," *Journal of Sound and Vibration*, vol. 320, pp. 125–144, 2009.

[4] H. Van der Auweraer, S. Donders, D. Hartmann, and W. Desmet, "Simulation and digital twin for mechatronic product design," in *Proceedings of ISMA2018 and USD2018*, Leuven, Belgium, 17-19 September 2018, pp. 3547–3566.

[5] D. De Gregoriis, P. Naets, F.and Kindt, and W. Desmet, "Development and validation of a fully predictive highfidelity simulation approach for predicting coarse road dynamic tire/road rolling contact forces," *Journal of Sound and Vibration*, vol. 452, pp. 147–168, 2019.

[6] J. Sanchez and H. Benaroya, "Review of force reconstruction techniques," *Journal of Sound and Vibration*, vol. 333, pp. 2999–3018, 2014.

[7] L. Jankowski, “Dynamic load identification for structural health monitoring,” Polish Academy of Science, Warsaw, Tech. Rep., 2013.

[8] D. Rixen and P. van der Valk, “An impulse based substructuring approach for impact analysis and load case simulations,” *Journal of Sound and Vibration*, no. 332, pp. 7174–7190, 2013.

[9] R. Kalman, “A new approach to linear filtering and prediction problems,” *J. Basic Eng.*, vol. 82, no. 1, pp. 35–45, 1960.

[10] R. Kalman and R. Bucy, “New results in linear filtering and prediction theory,” *J. Basic Eng.*, vol. 83, no. 3, pp. 95–180, 1961.

[11] J. Draper, S. Lee, and E. Marineau, “Numerical construction of impulse response functions and input signal reconstruction,” *Journal of Sound and Vibration*, vol. 432, pp. 259–271, 2018.

[12] A. K. Amiri and C. Bucher, “Derivation of a new parameteric impulse response matrix utilized for nodal wind load identification by response measurement,” *Journal of Sound and Vibration*, no. 334, pp. 101–113, 2015.

[13] T. Uhl, “The inverse identification problem and its technical application,” *Archive of Applied Mechanics*, vol. 77, no. 5, pp. 325–337, 2007.

[14] A. Tikhonov and V. Arsenin, *Solution of Ill-Posed Problems*. New York: Weily, 1977.

[15] B. Friedland, “Treatment of bias in recursive filtering,” *IEEE Trans. Autom. Control*, vol. 14, no. 4, pp. 359–367, 1969.

[16] E. Lourens, E. Reynders, G. De Roeck, G. Degrande, and G. Lombaert, “An augmented kalman filter for force identification in structural dynamics,” *Mechanical Systems and Signal Processing*, vol. 27, pp. 446–460, 2012.

[17] D. Simon, *Optimal State Estimation Kalman, Hinf, and Nonlinear Approaches*. New York: John Wiley and sons, 2006.

[18] C. Van Loan, “Computing integrals involving the matrix exponential,” *IEEE Transactions on Automatic Control*, vol. 23, no. 3, pp. 395–404, 1978.

[19] D. D. Gregoriis, F. Naets, P. Kindt, and W. Desmet, “Development and validation of a fully predictive high-fidelity simulation approach for predicting coarse road dynamic tire/road rolling contact forces,” *Journal of Sound and Vibration*, no. 452, pp. 147–168, 2019.

[20] D. De Gregoriis, F. Naets, and W. Desmet, “Multi-expansion modal reduction: A pragmatic semi-a priori model order reduction approach for nonlinear structural dynamics,” *Int J Numer Methods Eng*, vol. 118, pp. 765–782, 2019.

[21] M. Aucejo, O. De Smet, and J. Deu, “Practical issues on the applicability of kalman filtering for reconstructing mechanical sources in structural dynamics,” *Journal of Sound and Vibration*, vol. 442, pp. 45–70, 2019.

[22] F. Naets, J. Cuadrado, and W. Desmet, “Stable force identification in structural dynamics using kalman filtering and dummy-measurements,” *Mechanical Systemns and Signal Processing*, vol. 50-51, pp. 235–248, 2015.

[23] O. Bruls and A. M., “The generalized-alpha scheme as a linear multistep integrator: towards a general mechatronic simulator,” *ASME J Comput Nonlinear Dyn*, vol. 3, no. 4, 2008.